Advances in Nano Research, *Vol. 9, No. 3 (2020) 147-156*
DOI: https://doi.org/10.12989/anr.2020.9.3.147

Geometrical imperfection and thermal effects on nonlinear stability of microbeams made of graphene-reinforced nano-composites

Raad M. Fenjan, Nadhim M. Faleh and Ridha A. Ahmed*

Al-Mustansiriah University, Engineering Collage P.O. Box 46049, Bab-Muadum, Baghdad 10001, Iraq

(*Received September 6, 2019, Revised August 5, 2020, Accepted August 6, 2020*)

Abstract. This research is related to nonlinear stability analysis of advanced microbeams reinforced by Graphene Platelets (GPLs) considering generic geometrical imperfections and thermal loading effect. Uniform, linear and nonlinear distributions of GPLs in transverse direction have been considered. Imperfection sensitivity of post-bucking behaviors of the microbeam to different kinds of geometric imperfections have been examined. Geometric imperfection is first considered to be identical as the first buckling mode, then a generic function is employed to consider sine-type, local-type and global-type imperfectness. Modified couple stress theory is adopted to incorporate size-dependent behaviors of the beam at micro scale. The post-buckling problem is solved analytically to derive load-amplitude curves. It is shown that post-buckling behavior of microbeam is dependent on the type geometric imperfection and its magnitude. Also, post-buckling load can be enhanced by adding more GPLs or selecting a suitable distribution for GPLs.

Keywords: nonlinear stability; thermal load; graphene platelets; modified couple stress theory; nano-composite

1. Introduction

In recent years, different carbon structures including carbon nanotubes and carbon fibers are extensively applied in composite materials to enhance their thermal and mechanical characteristics (Yazid *et al.* 2018, Mokhtar *et al*. 2018, Besseghier *et al.* 2015, Chemi *et al.* 2015, Rakrak *et al*. 2016, Bensattalah *et al.* 2018). An increase of about 273% in elastic moduli of a carbon reinforced composite compared with a traditional composite has been reported by Ahankari and Kar (2010). Also, Gojny *et al*. (2004) stated that the stiffness of carbon reinforced composite can be increased even by embedding a small amount of carbon nanotubes. The effects of shape and size of carbon nanotubes on stiffness enhancement of composite materials with metal matrix have been investigated by Esawi *et al*. (2011). Due to having such superior characteristics, structural elements (beams and plates) having embedded nano-size carbon tubes have been researched in the view of their static and dynamic behaviors (Fantuzzi *et al*. 2017, Civalek 2017, Aragh 2017, Moradi-Dastjerdi and Malek-Mohammadi 2017, Kheroubi *et al*. 2016). However, graphene reinforced composites have been recently attracted huge attention due to their easier production approach and excellent stiffness enhancement mechanism. A review of different graphene nanoplate reinforced composites having ceramic and metal matrices has been represented by Nieto *et al.* (2017). A multi-scale analysis of mechanical characteristics of graphene nanoplate reinforced composites is presented by Lin *et al*. (2018) using finite element method. A report on the enhancement of thermal and mechanical character of graphene-reinforced composites has been presented by Wang *et al*. (2011).

Recently, many papers are published for investigating mechanical attributes of graphene based composite structures. Kitipornchai *et al.* (2017) studied stability as well as vibrational properties of porosity-dependent beams containing graphene-based composites. Furthermore, Feng *et al.* (2017) researched large amplitude vibrations of ideal Timoshenko beams with non-uniformly diffused graphene-based composites. Investigations on deflections of trapezoidal plate structures reinforced with functional gradation of graphene composites have been carried out by Zhao *et al.* (2017). Barati and Zenkour (2018a) researched vibrational attributes of graphene-based shells based on Galerkin's approach. Finite elements approach is used by Reddy *et al.* (2018) to explore vibrational attributes of a laminated graphene-based plate. Geometrically nonlinear vibrational attributes of scale-dependent beams made of graphene-based composites are researched by Sahmani and Aghdam (2017).

Micro/nano beams possess different mechanical characteristics from macro scale beams due to the fact that their mechanical behaviors are size-dependent (Bouafia *et al*. 2017, Mouffoki *et al*. 2017, Barati 2017, Semmah *et al*. 2014). Two particles at micro scale exert couple stress to each other leading to their micro-rotations. The most familiar theory capturing such micro-rotations is known as modified couple stress theory which has one scale factor (Park and Gao 2006, Barati and Zenkour 2018b). The scale parameter can be evaluated based on experiments (Lam *et al*. 2003, Tang and Alici 2011, Lei *et al.* 2016, Liebold and Müller 2016, Li *et al.* 2019a, b, Wi and Sodemann 2019).

*Corresponding author, Professor,
E-mail: dr.nadhim@uomustansiriyah.edu.iq

ISSN: 2287-237X (Print), 2287-2388 (Online)

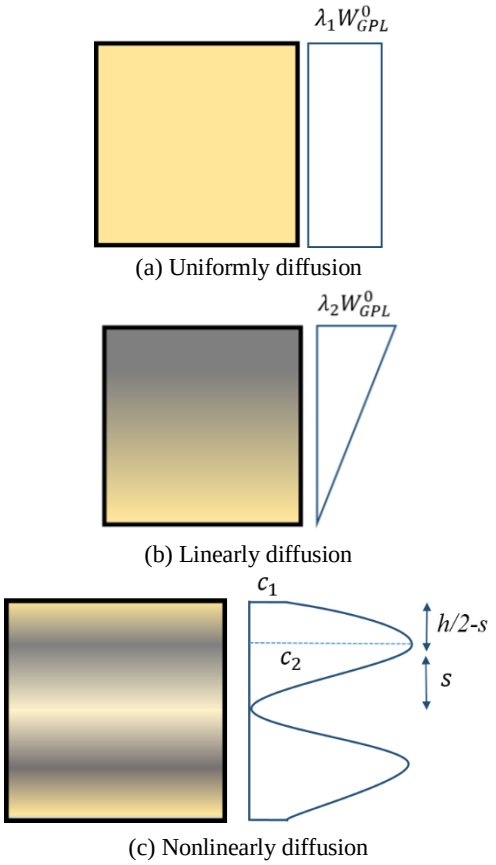

(a) Uniformly diffusion

(b) Linearly diffusion

(c) Nonlinearly diffusion

Fig. 1 Graphene diffusions in material structure

This theory is broadly used for examining vibrational and buckling characteristics of microbeams, but less studies are devoted to analysis of graphene platelet reinforced microbeams. Shenas *et al*. (2018) presented free vibrational analysis of shear deformable microbeams on elastic foundation with carbon nanotube fillers. Forced vibrational characteristics of a microbeams having embedded CNTs has been studied by Rostami *et al*. (2018) employing modified couple stress elasticity. Also, Mohammadimehr *et al*. (2017) researched free/forced vibrational behaviors of CNT reinforced micro-scale beams including viscoelasticity impacts. An analysis of vibration behavior of curved carbon nanotube reinforced micro-scale beams accounting for couple stress effects has been performed by Allahkarami and Nikkhah-Bahrami (2018). All of these works related to microbeams with embedded nanofillers studied a perfect microbeam neglecting geometric imperfections. Because of different fabrication and environmental parameters, geometrical imperfectness of an engineering structure, such as a beam, are inevitably created during the fabrication procedure (Wu *et al*. 2016, Barati and Zenkour 2018c).

Geometric imperfections can be regarded as two cases. In first case, the geometric imperfectness is identical to the first mode shape of microbeam. In second case, different imperfections of sine-type, local-type and global-type can be included using a general function. In this research, nonlinear stability analysis of microbeams on elastic foundation reinforced by Graphene Platelets (GPLs) considering above mentioned geometrical imperfections has

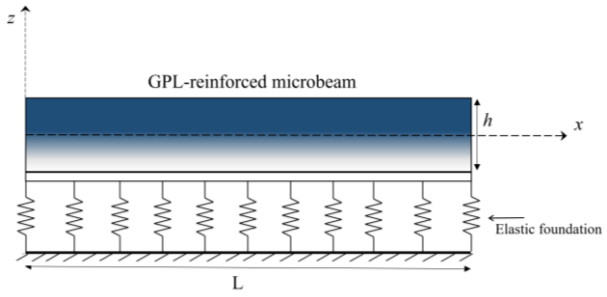

Fig. 2 Continuously graded graphene-reinforced microbeam

been carried out. Uniform, linear and nonlinear distributions of GPLs in transverse direction have been considered. Modified couple stress theory has been adopted to incorporate size-dependent behaviors of the beam at micro scale. The post-buckling problem is solved analytically to derive load-amplitude curves. It is illustrated that post-buckling path of a microbeam is dependent on the geometric imperfection type, imperfection amplitude, couple stress parameter and GPL reinforcement scheme.

2. Graphene based composites

According to Fig. 1, it is assumed that GPLs have three patterns of dispersal in the structure which includes uniform, linear and nonlinear. According to Fig. 2, a graphene reinforced composite micro-scale beam is illustrated. Micro-mechanic theory of such composite materials (Barati and Zenkour 2018a) introduces the below relationship between graphene platelets weight fraction (W_{GPL}) and their volume fraction (V_{GPL}) by

$$V_{GPL} = \frac{W_{GPL}}{W_{GPL} + \frac{\rho_{GPL}}{\rho_M} - \frac{\rho_{GPL}}{\rho_M} W_{GPL}} \tag{1}$$

so that ρ_{GPL} and ρ_M respectively define the mass densities of graphene and polymeric matrices. Next, the Young modulus of a graphene-based composite might be represented based upon matrix elastic modulus (E_M) by Barati and Zenkour (2018a)

$$E_1 = \frac{3}{8}\left(\frac{1+\xi_L^{GPL}\eta_L^{GPL}V_{GPL}}{1-\eta_L^{GPL}V_{GPL}}\right)E_M + \frac{5}{8}\left(\frac{1+\xi_W^{GPL}\eta_W^{GPL}V_{GPL}}{1-\eta_W^{GPL}V_{GPL}}\right)E_M \tag{2}$$

so that ξ_L^{GPL} and ξ_W^{GPL} define two geometrical factors indicating the impacts of graphene configuration and scales as Barati and Zenkour (2018a)

$$\xi_L^{GPL} = \frac{2l_{GPL}}{t_{GPL}} \tag{3a}$$

$$\eta_L^{GPL} = \frac{(E_{GPL}/E_M) - 1}{(E_{GPL}/E_M) + \xi_L^{GPL}} \tag{3b}$$

$$\xi_W^{GPL} = \frac{2w_{GPL}}{t_{GPL}} \tag{3c}$$

$$\eta_W^{GPL} = \frac{(E_{GPL}/E_M) - 1}{(E_{GPL}/E_M) + \xi_W^{GPL}} \tag{3d}$$

so that w_{GPL}, l_{GPL} and t_{GPL} define platelets mean widths, length, and thickness, respectively. Furthermore, Poisson's ratio for graphene-based composite might be defined based upon Poisson's ratio of the two constituents in the form

$$\begin{matrix} v_1 = v_{GPL}V_{GPL} + v_M V_M \\ \alpha_1 = \alpha_{GPL}V_{GPL} + \alpha_M V_M \end{matrix} \tag{4}$$

in which $V_M = 1 - V_{GPL}$ expresses the volume fractions of matrix component. Herein, three dispersions of the platelets have been assumed as:

Uniform:

$$W_{GPL} = \lambda_1 W_{GPL}^0 \tag{5a}$$

Linear:

$$W_{GPL} = \lambda_2 W_{GPL}^0 (\frac{z}{h} + \frac{1}{2}) \tag{5b}$$

Nonlinear:

$$W_{GPL} = \frac{\lambda_3 W_{GPL}^0 z^2}{s^2 h^2 (4s^2 - h^2)} \left[4h^2 z^2 - h^4 + \frac{16s^2}{n}(s^2 - z^2) \right] \tag{5c}$$
$$s = 0.45h$$

where $W_{GPL}^0 = 1\%$ expresses a particular weight fraction for graphene platelets.

The classical microbeam with embedded graphene nanofillers is considered to have a displacement field as

$$u_1(x,z) = u(x) - z\frac{\partial w}{\partial x} \tag{6a}$$

$$u_3(x,z) = w(x) \tag{6b}$$

where *u* and *w* respectively represent the axial and lateral displacements. The only non-zero strain is axial strain containing moderate deformations as Emam (2009)

$$\begin{matrix} \varepsilon_x = \frac{\partial u}{\partial x} + \frac{1}{2}[(\frac{\partial w}{\partial x})^2 - (\frac{\partial w^*}{\partial x})^2] - z(\frac{\partial^2 w}{\partial x^2} - \frac{\partial^2 w^*}{\partial x^2}) \\ \gamma_{xz} = 0 \end{matrix} \tag{7}$$

in which w^* is the initial deflection of the microbeam due to geometric imperfections. Also, the components of curvature tensor may be defined as

$$\begin{matrix} \chi_{xy} = -\frac{1}{2}\frac{\partial^2 w}{\partial x^2} \\ \chi_{xx} = \chi_{yy} = \chi_{zz} = \chi_{xz} = \chi_{yz} = 0 \end{matrix} \tag{8}$$

The classical stress-strain and couple stress-curvature relations for a microbeam can be expressed as

$$\sigma_{xx} = E_1 \varepsilon_{xx} \tag{9}$$

$$m_{xy} = 2Gl^2 \chi_{xy} \tag{10}$$

in which E_1 and G define Young's modulus and shear modulus of the nanocomposite, respectively.

It must be stated that the one-dimensional stress-strain relationship is used. However, it is recently reported that Poisson effect can be included in analysis of micro-scale beams based on a three-dimensional stress-strain relationship (Ma *et al*. 2008). But, Dehrouyeh-Semnani and Nikkhah-Bahrami (2015) reported that three-dimensional stress-strain model is not appropriate and the one-dimensional stress-strain model must be utilized. Also, this study neglects shear deformation effect due to employment of classic beam theory. The governing equations for a beam might be obtained by maximization of the total potential energy as (Emam 2009)

$$\frac{\partial N_x}{\partial x} = 0 \tag{11}$$

$$\frac{\partial^2 M_x^b}{\partial x^2} + \frac{\partial^2 Y_1}{\partial x^2} = -\frac{\partial}{\partial x}(N_x \frac{\partial w}{\partial x}) + k_L w - k_P \nabla^2 w + k_{NL} w^3 \tag{12}$$

so that k_L, k_p and k_{NL} define elastic substrate coefficients. Also, force and moment resultants may be defined by

$$N_x = A[\frac{\partial u}{\partial x} + \frac{1}{2}(\frac{\partial w}{\partial x})^2 - \frac{1}{2}(\frac{\partial w^*}{\partial x})^2] - B(\frac{\partial^2 w}{\partial x^2} - \frac{\partial^2 w^*}{\partial x^2}) - N^T \tag{13}$$

$$M_x^b = B[\frac{\partial u}{\partial x} + \frac{1}{2}(\frac{\partial w}{\partial x})^2 - \frac{1}{2}(\frac{\partial w^*}{\partial x})^2] - D(\frac{\partial^2 w}{\partial x^2} - \frac{\partial^2 w^*}{\partial x^2}) \tag{14}$$

$$Y_1 = -\tilde{A}(\frac{\partial^2 w}{\partial x^2} - \frac{\partial^2 w^*}{\partial x^2}) \tag{15}$$

where N^T is exerted thermal load: $N^T = \int_{-h/2}^{h/2} E_1 \alpha_1 \Delta T dz$ and ΔT is temperature rise

$$\begin{matrix} A = \int_{-h/2}^{h/2} E_1 \, dz, B = \int_{-h/2}^{h/2} E_1 z \, dz \\ D = \int_{-h/2}^{h/2} E_1 z^2 \, dz \\ \tilde{A} = \int_{-h/2}^{h/2} G l^2 \, dz \end{matrix} \tag{16}$$

Finally, the governing equations for an imperfect microbeam with respect to displacement components can be obtained by inserting Eqs. (13)-(15) into Eqs. (11)-(12) as

$$A(\frac{\partial^2 u}{\partial x^2}) - B(\frac{\partial^3 w}{\partial x^3} - \frac{\partial^3 w^*}{\partial x^3}) + A(\frac{\partial w}{\partial x}\frac{\partial^2 w}{\partial x^2} - \frac{\partial w^*}{\partial x}\frac{\partial^2 w^*}{\partial x^2}) = 0 \tag{17}$$

$$\begin{matrix} B\frac{\partial}{\partial x}\left(\frac{\partial^2 u}{\partial x^2} + \frac{\partial w}{\partial x}\frac{\partial^2 w}{\partial x^2} - \frac{\partial w^*}{\partial x}\frac{\partial^2 w^*}{\partial x^2}\right) - (D + \tilde{A}) \\ \times \left(\frac{\partial^4 w}{\partial x^4} - \frac{\partial^4 w^*}{\partial x^4}\right) + \frac{\partial}{\partial x}\left(N_x \frac{\partial w}{\partial x}\right) - k_L(w - w^*) \\ + k_P \nabla^2 (w - w^*) - k_{NL}(w - w^*)^3 = 0 \end{matrix} \tag{18}$$

Using Eq. (17) and discarding thermal effects, one can get to

$$\frac{\partial}{\partial x}\left(A\frac{\partial u}{\partial x}+\frac{A}{2}(\frac{\partial w}{\partial x})^2-\frac{A}{2}(\frac{\partial w^*}{\partial x})^2-B(\frac{\partial^2 w}{\partial x^2}-\frac{\partial^2 w^*}{\partial x^2})\right)=0 \quad (19)$$

The following conclusion can be made from Eq. (19)

$$\frac{\partial u}{\partial x}=-\frac{1}{2}(\frac{\partial w}{\partial x})^2+\frac{1}{2}(\frac{\partial w^*}{\partial x})^2+\frac{B}{A}(\frac{\partial^2 w}{\partial x^2}-\frac{\partial^2 w^*}{\partial x^2})+\frac{c_1}{A} \quad (20)$$

Then, integration from Eq. (20) gives

$$\begin{aligned} u=&-\frac{1}{2}\int_0^x(\frac{\partial w}{\partial x})^2\,dx+\frac{1}{2}\int_0^x(\frac{\partial w^*}{\partial x})^2\,dx\\ &+\frac{B}{A}(\frac{\partial w}{\partial x}-\frac{\partial w^*}{\partial x})+\frac{c_1}{A}x+c_2 \end{aligned} \quad (21)$$

Imposing axial boundary condition ($u(0) = 0$, $u(L) = -PL/A$) of the microbeam into Eq. (21) gives two constants c_1 and c_2 as

$$\begin{aligned} c_2=&-\frac{B}{A}\left(\frac{\partial w}{\partial x}-\frac{\partial w^*}{\partial x}\right)|x=0\\ c_1=&-P+\frac{A}{2L}\int_0^L(\frac{\partial w}{\partial x})^2\,dx-\frac{A}{2L}\int_0^L(\frac{\partial w^*}{\partial x})^2\,dx\\ &-\frac{B}{L}(\frac{\partial w}{\partial x}-\frac{\partial w^*}{\partial x})|x=L+\frac{B}{L}(\frac{\partial w}{\partial x}-\frac{\partial w^*}{\partial x})|x=0 \end{aligned} \quad (22)$$

Inserting two constants from Eq. (22) into Eq. (20) give the first derivative of axial displacement as

$$\begin{aligned} \frac{\partial u}{\partial x}=&-\frac{1}{2}(\frac{\partial w}{\partial x})^2+\frac{1}{2}(\frac{\partial w^*}{\partial x})^2+\frac{B}{A}(\frac{\partial^2 w}{\partial x^2}-\frac{\partial^2 w^*}{\partial x^2})-\frac{P}{A}\\ &+\frac{1}{2L}\int_0^L(\frac{\partial w}{\partial x})^2\,dx-\frac{1}{2L}\int_0^L(\frac{\partial w^*}{\partial x})^2\,dx-\frac{B}{LA}\\ &\times(\frac{\partial w_b}{\partial x}-\frac{\partial w_b^*}{\partial x})|x=L+\frac{B}{LA}(\frac{\partial w_b}{\partial x}-\frac{\partial w_b^*}{\partial x})|x=0 \end{aligned} \quad (23)$$

In Eq. (23), taking derivatives with respect to x gives the following relations

$$\frac{\partial^2 u}{\partial x^2}=-\frac{\partial w}{\partial x}\frac{\partial^2 w}{\partial x^2}+\frac{\partial w^*}{\partial x}\frac{\partial^2 w^*}{\partial x^2}+\frac{B}{A}(\frac{\partial^3 w}{\partial x^3}-\frac{\partial^3 w^*}{\partial x^3}) \quad (24)$$

$$\begin{aligned} \frac{\partial^3 u}{\partial x^3}=&-(\frac{\partial^2 w}{\partial x^2})^2-\frac{\partial w}{\partial x}\frac{\partial^3 w}{\partial x^3}+(\frac{\partial^2 w^*}{\partial x^2})^2+\frac{\partial w^*}{\partial x}\frac{\partial^3 w^*}{\partial x^3}\\ &+\frac{B}{A}(\frac{\partial^4 w}{\partial x^4}-\frac{\partial^4 w^*}{\partial x^4}) \end{aligned} \quad (25)$$

Eqs. (23)-(25) must be inserting into Eq. (18) to obtain the governing equation in its final form

$$\begin{aligned} &\frac{B^2}{A}(\frac{\partial^4 w}{\partial x^4}-\frac{\partial^4 w^*}{\partial x^4})+A[-\frac{P}{A}+\frac{1}{2L}\int_0^L(\frac{\partial w}{\partial x})^2\,dx\\ &-\frac{1}{2L}\int_0^L(\frac{\partial w^*}{\partial x})^2\,dx-\frac{B}{LA}\left(\frac{\partial w}{\partial x}-\frac{\partial w^*}{\partial x}\right)|x=L\\ &+\frac{B}{LA}(\frac{\partial w}{\partial x}-\frac{\partial w^*}{\partial x})|x=0]\frac{\partial^2 w}{\partial x^2}-k_L(w-w^*)\\ &+k_P\nabla^2(w-w^*)-k_{NL}(w-w^*)^3\\ &-(D+\tilde{A})(\frac{\partial^4 w}{\partial x^4}-\frac{\partial^4 w^*}{\partial x^4})=0 \end{aligned} \quad (26)$$

3. Solution approach

The nonlinear stability equations of an imperfect microbeam have been analytically solved within the present chapter. The transverse field component has been presented in the form (Ebrahimi and Barati 2017, Hadji *et al.* 2015)

$$w=\sum_{i=1}^{\infty}W_i\varphi_i(x) \quad (27)$$

where W_i is the buckling deflection and $\varphi_i(x)=0.5(1-cos\left(\frac{2i\pi}{L}x\right))$ defines a test function for satisfying clamped boundary condition having the below form

$$\begin{aligned} &w|x=0=w|x=L=0\\ &\frac{\partial w}{\partial x}|x=0=\frac{\partial w}{\partial x}|x=L=0 \end{aligned} \quad (28)$$

As mentioned in the text, two cases of geometric imperfection have been considered.

1: The geometric imperfectness is identical as first buckling configuration.

$$w^*=W^*\Phi=0.5W^*\left(1-cos\left(2\pi\frac{x}{L}\right)\right) \quad (29)$$

2: The geometric imperfectness is sine-type, local-type or global-type described via the following generic function

$$w^*=W^*\,sech\left[a\left(\frac{x}{L}-c\right)\right]cos\left[\pi b\left(\frac{x}{L}-c\right)\right] \quad (30)$$

where a, b and c are constants and W^* is the mid-span initial rise.

Finally, placing Eqs. (27)-(30) into the governing equation yield the following simple equation as

$$\widetilde{K}\widetilde{W}+G^*\widetilde{W}^3+\Gamma\widetilde{W}^2+\Psi W^*=0 \quad (31)$$

in which $\widetilde{W}$ is the maximum amplitude. Also, $\widetilde{K}$ is linear stiffness matrix. G^* and Γ are nonlinear stiffness matrix which can be calculated using Galerkin's method. Also, some parameters are normalized as

$$\begin{aligned} &K_L=k_L\frac{L^4}{D},\qquad K_p=k_p\frac{L^2}{D}\\ &K_{NL}=k_{NL}\frac{L^4}{A},\qquad \widetilde{W}=W/h \end{aligned} \quad (32)$$

4. Results and discussions

Post-buckling path obtained in section 3 are illustrated and discussed in several figures of present section. Results are presented accounting for 3 cases of GPL dispersions which are uniform, linear and nonlinear. Tables 1 and 2 represent material properties of the micro-size beam. Four kinds of geometric imperfections for the microbeam have been considered. Two functions are introduced to describe various geometric imperfection. A trigonometric function

Table 1 Influence of gradient index on the amount of GPL

Uniform (λ_1)	Linear (λ_2)	Nonlinear (λ_3)	% W^*_{GPL}
0	0	0	0
0.33	0.67	0.43	0.33
1	2	1.29	1

Table 2 Material and geometric factors of the GPL-reinforced composites

GPLs	Matrix (Epoxy resin)
E_{GPL} = 1.01 TPa	E_M = 2.85 GPa
ρ_{GPL} = 1062.5 kg/m^3	ρ_M = 1200 kg/m^3
v_{GPL} = 0.006	v_M = 0.34
t_{GPL} = 1.5 nm	-
w_{GPL} = 1.5 μm	-
l_{GPL} = 2.5 μm	-

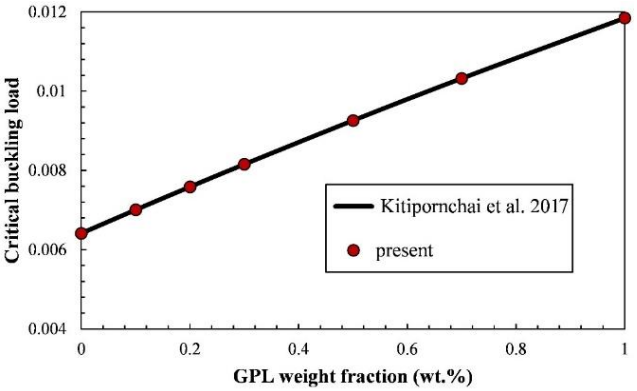

Fig. 3 Validating the non-dimension buckling load of GPL-reinforced beam (L/h = 20)

has been considered for describing the geometric imperfectness identical to 1st buckling mode. Also, the generic function is employed to consider sine-type, local-type and global-type imperfectness.

To examine the accuracy of solution method and also modeling of nano-composite material, a comparison between obtained static buckling loads with those obtained by Kitipornchai *et al*. (2017) for a variety of GPL weight fraction has been presented in Fig. 3. This figure shows that the presented finite element solution is in excellent agreement with analytical results provided by Kitipornchai *et al*. (2017). Also, post-buckling loads of a multi-layered GPL-reinforced beam are validated with those of Yang *et al*. (2017) and the results are provided in Table 3.

In Fig. 4, post-buckling load-amplitude curves of a GPL-reinforced microbeam having clamped boundary conditions with and without geometric imperfections have been presented accounting for various GPL weight fraction and dispersions. It is considered that L/h = 20, K_w = 0, K_p = 0, W^* = 0.01 h and l/h = 0.2. First, it must be mentioned that obtained load for a perfect microbeam at $\widetilde{W}/h$ = 0 is the critical buckling load. For microbeams having

Table 3 Comparison of post-buckling load for a multi-layered GPL reinforced beam (W_{GPL} = 0.3%, $\widetilde{W}/h$ = 1)

Number of layers	Yang *et al*. (2017)	Present
4	0.1175	0.1174
6	0.1192	0.1190
10	0.1201	0.1200
28	0.1205	0.1205

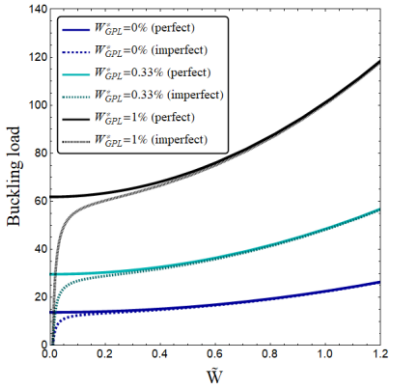

(a) Uniformly dispersed GPLs

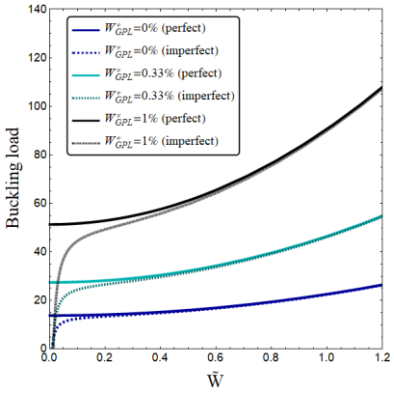

(b) Linearly dispersed GPLs

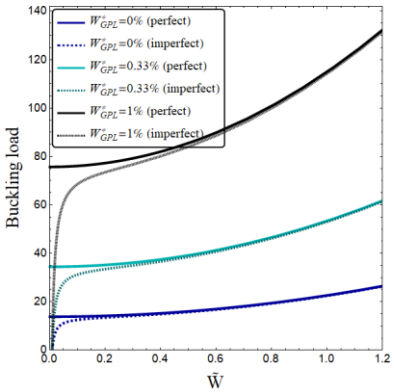

(c) Nonlinearly dispersed GPLs

Fig. 4 Nonlinear buckling load against dimensionless amplitude for various GPL distributions and weight fractions (L/h = 20, K_w = 0, K_p = 0, W^* = 0.01 h, l/h = 0.2)

geometric imperfection there is not critical buckling load

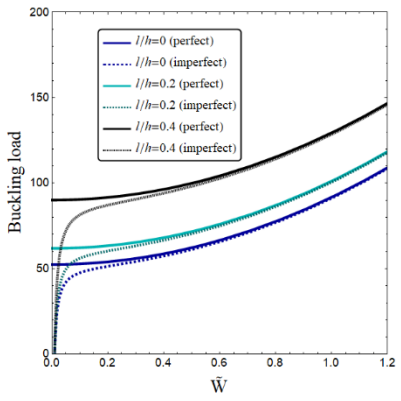

(a) Uniformly dispersed GPLs

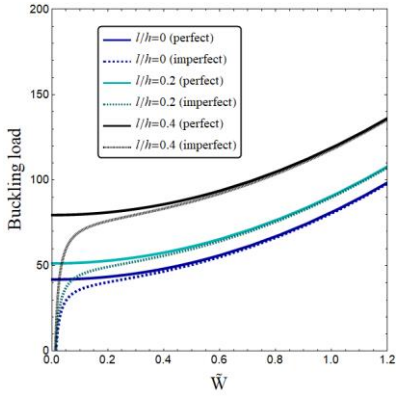

(b) Linearly dispersed GPLs

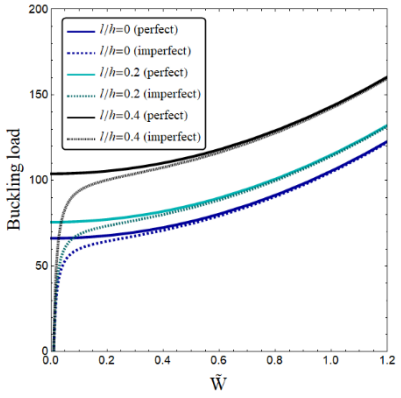

(c) Nonlinearly dispersed GPLs

Fig. 5 Nonlinear buckling load against dimensionless amplitude for various GPL distributions and couple stress parameters (L/h = 20, K_w = 0, K_p = 0, W^* = 0.01 h, W^*_{GPL} = 1%)

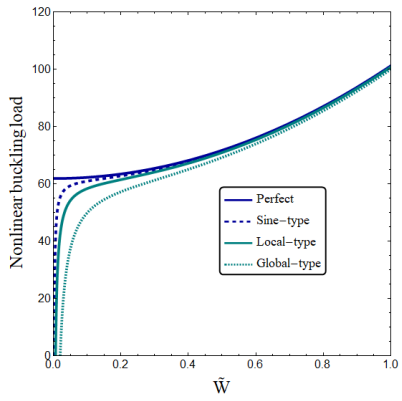

(a) Uniformly dispersed GPLs

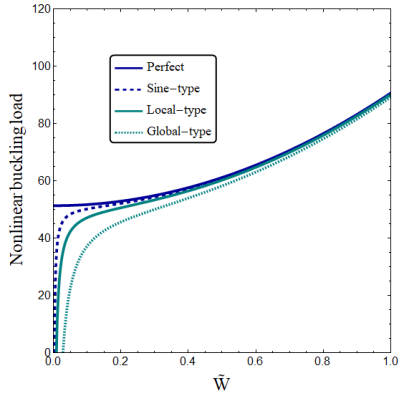

(b) Linearly dispersed GPLs

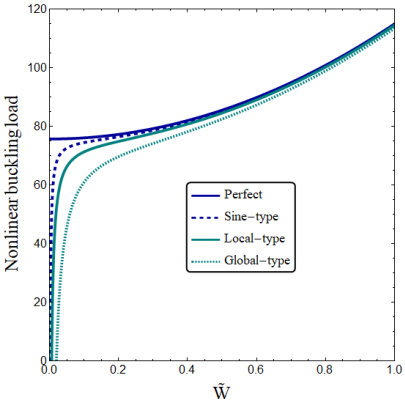

(c) Nonlinearly dispersed GPLs

Fig. 6 Nonlinear buckling load against dimensionless amplitude for various GPL distribution and geometric imperfections (L/h = 20, K_w = 0, K_p = 0, W^* = 0.01 h, W^*_{GPL} = 1%)

since they are at their initial geometry when $\widetilde{W}/h$ = 0. However, increasing $\widetilde{W}/h$ = 0 results in higher post-buckling loads due to inclusion of hardening effects. The most important observation from this figure is that increasing GPL weight fraction yields larger buckling loads for all types of GPL distributions. It means that adding the amount of GPLs can increase the microbeam stiffness and enhance its post-buckling behavior. Also, the maximum and minimum post-buckling loads are obtained for nonlinear and linear GPL distributions respectively. In the case of linear dispersion, the amount of GPLs are maximum at upper side of microbeam and zero at bottom side. That's the reason why linear GPL distribution gives smaller buckling loads compared with uniform distribution.

Small scale effects on nonlinear stability behavior of perfect/imperfect GPL-reinforced microbeams have been illustrated in Fig. 5 in the context of modified couple stress theory. Geometric imperfectness has been considered as the 1st mode shape of microbeam and has the magnitude of W^* = 0.01 h. Again, results are presented for different distributions of GPLs when the weight fraction is set to W^*_{GPL} = 1%. It is well-known that couple stress effect accounts for the particle rotations at micron size. Increasing couple stress parameter exerts a hardening effect to the

microbeam leading to larger post-buckling loads for both perfect and imperfect microbeams. The zero value for couple stress parameter means that small scale effects are ignored.

Impacts of generic geometric imperfectness on nonlinear stability curves of the microbeam are shown in Fig. 6 at $W^* = 0.01\ h$. In fact, three cases of sine-type, local-type and global-type imperfections have been included instead of considering the imperfection identical to first buckling mode. Different distributions of graphene platelets with $W^*_{GPL} = 1\%$ are also considered. One can see that the difference among buckling loads of perfect and imperfect microbeams is very small at large dimensionless amplitudes ($\widetilde{W}/h$). So, geometric imperfections are more important at small amplitudes. Among considered imperfections, sine-type imperfection gives largest buckling loads and global-type imperfection leads to smallest buckling loads. The most difference among perfect and imperfect microbeams is obtained in the case of global-type imperfection.

Nonlinear buckling load against non-dimension amplitude for various foundation parameters and geometric imperfections is demonstrated in Fig. 7 when L/h = 20. Uniform GPL distribution with $W^*_{GPL} = 1\%$ is considered for this example. The geometric imperfectness has been considered to be the same as 1st buckling mode. The amplitude of imperfectioness is set as $W^* = 0.01\ h$ in this figure. All foundation factors yield larger post-buckling loads. It is evident that nonlinear layer of elastic foundation (K_{NL}) has no effect on buckling load at small amplitudes while its effect becomes more announced at large amplitudes. So, it can be concluded that the effect of nonlinear layer is amplitude dependent. But, the effects of linear layer (K_L) and Pasternak layer (K_P) are independent of amplitude.

Fig. 8 examines the influences of slenderness ration (L/h) on nonlinear stability curves of a GPL-reinforced microbeam. Geometric imperfectness has been included as the 1st mode shape of micro-size beam and has the magnitude of $W^* = 0.01\ h$. Uniform GPL distribution with $W^*_{GPL} = 1\%$ is considered for this example. A microbeam with higher slenderness ratios is more flexible and has smaller buckling loads. So, increasing the value of slenderness ration reduces the magnitude of post-buckling load. Such finding is correct for both perfect and imperfect microbeams.

The nonlinear buckling load of a GPL-reinforced microbeam versus dimensionless amplitude for various imperfection amplitudes has been illustrated in Fig. 9 at $L/h = 20$ and $l/h = 0.2$. In this figure, the first buckling mode is considered as geometric imperfection. The weight fraction of uniform GPLs is set as $W^*_{GPL} = 1\%$. Increasing the magnitude of geometric imperfection amplitude results in smaller buckling loads. It means that larger imperfections make the microbeam more sensitive to applied loads. For all values of geometric imperfection amplitude, the post-buckling load rapidly increases from zero and becomes very close to the post-buckling load of a perfect microbeam. However, the difference between obtained post-buckling loads of different geometric imperfections becomes very small at large dimensionless amplitudes.

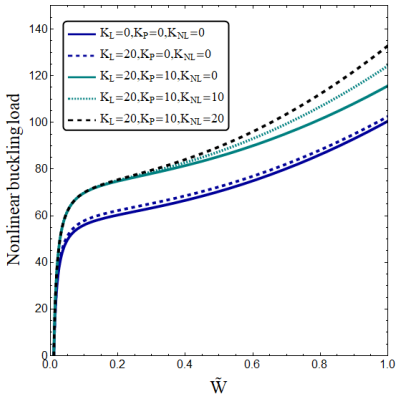

Fig. 7 Nonlinear buckling load against dimensionless amplitude for various foundation parameters and geometric imperfectness ($L/h = 20$, $W^* = 0.01\ h$, $W^*_{GPL} = 1\%$)

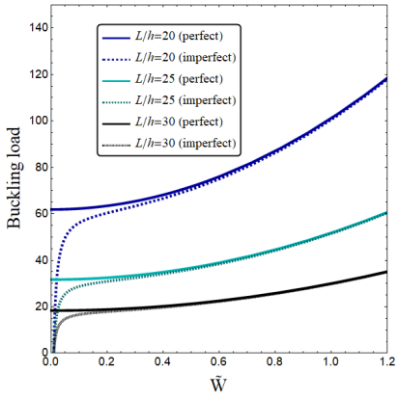

Fig. 8 Nonlinear buckling load against dimensionless amplitude for various slenderness ratios ($W^* = 0.01\ h$, $W^*_{GPL} = 1\%$)

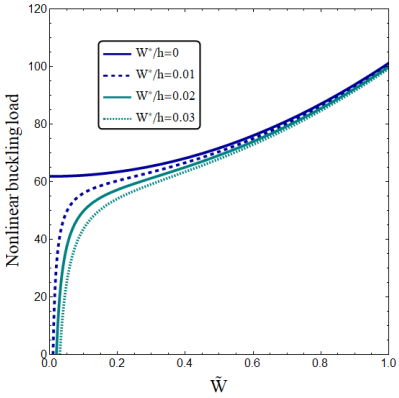

Fig. 9 Nonlinear buckling load against dimensionless amplitude for various imperfection amplitudes ($L/h = 20$, $l/h = 0.2$, $W^*_{GPL} = 1\%$)

Fig. 10 studies the influences of temperature rise (ΔT) on nonlinear stability curves of a GPL-reinforced microbeam. Geometric imperfectness has been included as the 1st mode shape of micro-size beam and has the magnitude of $W^* = 0.01$ h. Uniform GPL distribution with

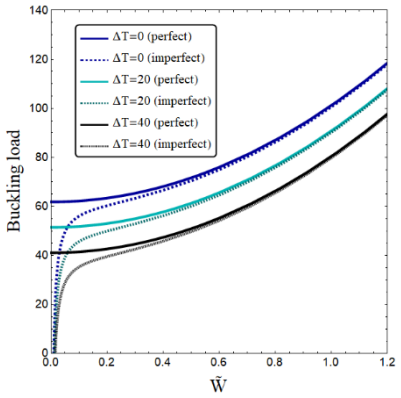

Fig. 10 Nonlinear buckling load against dimensionless amplitude for various temperature variation (L/h = 20, l/h = 0.2, W^*_{GPL} = 1%)

W^*_{GPL} = 1% is considered for this example. A microbeam under higher temperature rise is more flexible and has smaller buckling loads. So, increasing the value of temperature rise reduces the magnitude of post-buckling load.

5. Conclusions

As the first attempt, nonlinear stability problem of a geometrically imperfect microbeam reinforced by functionally graded graphene platelets was solved in this research. Three kinds of GPL distribution as well as four kinds of geometric imperfections were considered. The microbeam was embedded on a three-parameter elastic foundation having cubic nonlinearity. It was found that increasing GPL weight fraction yields larger buckling loads for all types of GPL distributions. Also, the maximum and minimum post-buckling loads were obtained for nonlinear and linear GPL distributions, respectively. Among considered imperfections, sine-type imperfection gave largest buckling loads and global-type imperfection led to smallest buckling loads. The most difference between perfect and imperfect microbeams was obtained in the case of global-type imperfection. Also, it was concluded that the effect of nonlinear layer of elastic foundation is amplitude dependent.

Acknowledgments

The authors would like to thank Mustansiriyah university (www.uomustansiriyah.edu.iq) Baghdad-Iraq for its support in the present work.

References

Ahankari, S.S. and Kar, K.K. (2010), "Hysteresis measurements and dynamic mechanical characterization of functionally graded natural rubber-carbon black composites", *Polym. Eng. Sci.*, **50**(5), 871-877. https://doi.org/10.1002/pen.21601.

Allahkarami, F. and Nikkhah-Bahrami, M. (2018), "The effects of agglomerated CNTs as reinforcement on the size-dependent vibration of embedded curved microbeams based on modified couple stress theory", *Mech. Adv. Mater. Struct.*, **25**(12), 995-1008. https://doi.org/10.1080/15376494.2017.1323144.

Aragh, B.S. (2017), "Mathematical modelling of the stability of carbon nanotube-reinforced panels", *Steel Compos. Struct., Int. J.*, **24**(6), 727-740. https://doi.org/10.12989/scs.2017.24.6.727.

Barati, M.R. (2017), "Coupled effects of electrical polarization-strain gradient on vibration behavior of double-layered flexoelectric nanoplates", *Smart Struct. Syst., Int. J.*, **20**(5), 573-581. https://doi.org/10.12989/sss.2017.20.5.573.

Barati, M.R. and Zenkour, A.M. (2018a), "Vibration analysis of functionally graded graphene platelet reinforced cylindrical shells with different porosity distributions", *Mech. Adv. Mater. Struct.*, **26**(18), 1580-1588. https://doi.org/10.1080/15376494.2018.1444235.

Barati, M.R. and Zenkour, A.M. (2018b), "Analysis of postbuckling behavior of general higher-order functionally graded nanoplates with geometrical imperfection considering porosity distributions", *Mech. Adv. Mater. Struct.*, **26**(12), 1081-1088. https://doi.org/10.1080/15376494.2018.1430280.

Barati, M.R. and Zenkour, A.M. (2018c), "Post-buckling analysis of imperfect multi-phase nanocrystalline nanobeams considering nanograins and nanopores surface effects", *Compos. Struct.*, **184**, 497-505. https://doi.org/10.1016/j.compstruct.2017.10.019.

Bensattalah, T., Bouakkaz, K., Zidour, M. and Daouadji, T.H. (2018), "Critical buckling loads of carbon nanotube embedded in Kerr's medium", *Adv. Nano Res., Int. J.*, **6**(4), 339-356. https://doi.org/10.12989/anr.2018.6.4.339.

Besseghier, A., Heireche, H., Bousahla, A.A., Tounsi, A. and Benzair, A. (2015), "Nonlinear vibration properties of a zigzag single-walled carbon nanotube embedded in a polymer matrix", *Adv. Nano Res., Int. J.*, **3**(1), 29-37. https://doi.org/10.12989/anr.2015.3.1.029.

Bouafia, K., Kaci, A., Houari, M.S.A., Benzair, A. and Tounsi, A. (2017), "A nonlocal quasi-3D theory for bending and free flexural vibration behaviors of functionally graded nanobeams", *Smart Struct. Syst., Int. J.*, **19**(2), 115-126. https://doi.org/10.12989/sss.2017.19.2.115.

Chemi, A., Heireche, H., Zidour, M., Rakrak, K. and Bousahla, A.A. (2015), "Critical buckling load of chiral double-walled carbon nanotube using non-local theory elasticity", *Adv. Nano Res., Int. J.*, **3**(4), 193-206. https://doi.org/10.12989/anr.2015.3.4.193.

Civalek, Ö. (2017), "Free vibration of carbon nanotubes reinforced (CNTR) and functionally graded shells and plates based on FSDT via discrete singular convolution method", *Compos. Part B Eng.*, **111**, 45-59. https://doi.org/10.1016/j.compositesb.2016.11.030.

Dehrouyeh-Semnani, A.M. and Nikkhah-Bahrami, M. (2015), "A discussion on incorporating the Poisson effect in microbeam models based on modified couple stress theory", *Int. J. Eng. Sci.*, **86**, 20-25. https://doi.org/10.1016/j.ijengsci.2014.10.003.

Emam, S.A. (2009), "A static and dynamic analysis of the postbuckling of geometrically imperfect composite beams", *Compos. Struct.*, **90**(2), 247-253. https://doi.org/10.1016/j.compstruct.2009.03.020.

Esawi, A.M.K., Morsi, K., Sayed, A., Taher, M. and Lanka, S. (2011), "The influence of carbon nanotube (CNT) morphology and diameter on the processing and properties of CNT-reinforced aluminium composites", *Compos. Part A Appl. Sci. Manuf.*, **42**(3), 234-243. https://doi.org/10.1016/j.compositesa.2010.11.008.

Fantuzzi, N., Tornabene, F., Bacciocchi, M. and Dimitri, R. (2017), "Free vibration analysis of arbitrarily shaped

functionally graded carbon nanotube-reinforced plates", *Compos. Part B Eng.*, **115**, 384-408. https://doi.org/10.1016/j.compositesb.2016.09.021.

Feng, C., Kitipornchai, S. and Yang, J. (2017), "Nonlinear free vibration of functionally graded polymer composite beams reinforced with graphene nanoplatelets (GPLs)", *Eng. Struct.*, **140**, 110-119. https://doi.org/10.1016/j.engstruct.2017.02.052.

Gojny, F.H., Wichmann, M.H.G., Köpke, U., Fiedler, B. and Schulte, K. (2004), "Carbon nanotube-reinforced epoxy-composites: enhanced stiffness and fracture toughness at low nanotube content", *Compos. Sci. Technol.*, **64**(15), 2363-2371. https://doi.org/10.1016/j.compscitech.2004.04.002.

Hadji, L., Daouadji, T.H. and Bedia, E.A. (2015), "A refined exponential shear deformation theory for free vibration of FGM beam with porosities", *Geomech. Eng., Int. J.*, **9**(3), 361-372. https://doi.org/10.12989/gae.2015.9.3.361.

Kheroubi, B., Benzair, A., Tounsi, A. and Semmah, A. (2016), "A new refined nonlocal beam theory accounting for effect of thickness stretching in nanoscale beams", *Adv. Nano Res., Int. J.*, **4**(4), 251-264. https://doi.org/10.12989/anr.2016.4.4.251.

Kitipornchai, S., Chen, D. and Yang, J. (2017), "Free vibration and elastic buckling of functionally graded porous beams reinforced by graphene platelets", *Mater. Des.*, **116**, 656-665. https://doi.org/10.1016/j.matdes.2016.12.061.

Lam, D.C., Yang, F., Chong, A.C.M., Wang, J. and Tong, P. (2003), "Experiments and theory in strain gradient elasticity", *J. Mech. Phys. Solids*, **51**(8), 1477-1508. https://doi.org/10.1016/S0022-5096(03)00053-X.

Lei, J., He, Y., Guo, S., Li, Z. and Liu, D. (2016), "Size-dependent vibration of nickel cantilever microbeams: Experiment and gradient elasticity", *AIP Adv.*, **6**(10), 105202. https://doi.org/10.1063/1.4964660.

Li, Z., He, Y., Lei, J., Han, S., Guo, S. and Liu, D. (2019a), "Experimental investigation on size-dependent higher-mode vibration of cantilever microbeams", *Microsyst. Technol.*, **25**(8), 3005-3015. https://doi.org/10.1007/s00542-018-4244-0.

Li, Z., He, Y., Zhang, B., Lei, J., Guo, S. and Liu, D. (2019b), "Experimental investigation and theoretical modelling on nonlinear dynamics of cantilevered microbeams", *Eur. J. Mech. A Solids*, **78**, 103834. https://doi.org/10.1016/j.euromechsol.2019.103834.

Liebold, C. and Müller, W.H. (2016), "Comparison of gradient elasticity models for the bending of micromaterials", *Comput. Mater. Sci.*, **116**, 52-61. https://doi.org/10.1016/j.commatsci.2015.10.031.

Lin, F., Yang, C., Zeng, Q.H. and Xiang, Y. (2018), "Morphological and mechanical properties of graphene-reinforced PMMA nanocomposites using a multiscale analysis", *Comput. Mater. Sci.*, **150**, 107-120. https://doi.org/10.1016/j.commatsci.2018.03.048.

Ma, H.M., Gao, X.L. and Reddy, J.N. (2008), "A microstructure-dependent Timoshenko beam model based on a modified couple stress theory", *J. Mech. Phys. Solids*, **56**(12), 3379-3391. https://doi.org/10.1016/j.jmps.2008.09.007.

Mohammadimehr, M., Monajemi, A.A. and Afshari, H. (2017), "Free and forced vibration analysis of viscoelastic damped FG-CNT reinforced micro composite beams", *Microsyst. Technol.*, **26**, 3085-3099. https://doi.org/10.1007/s00542-017-3682-4.

Mokhtar, Y., Heireche, H., Bousahla, A.A., Houari, M.S.A., Tounsi, A. and Mahmoud, S.R. (2018), "A novel shear deformation theory for buckling analysis of single layer graphene sheet based on nonlocal elasticity theory", *Smart Struct. Syst., Int. J.*, **21**(4), 397-405. http://dx.doi.org/10.12989/sss.2018.21.4.397.

Mouffoki, A., Bedia, E.A., Houari, M.S.A., Tounsi, A. and Mahmoud, S.R. (2017), "Vibration analysis of nonlocal advanced nanobeams in hygro-thermal environment using a new two-unknown trigonometric shear deformation beam theory", *Smart Struct. Syst., Int. J.*, **20**(3), 369-383. https://doi.org/10.12989/sss.2017.20.3.369.

Moradi-Dastjerdi, R. and Malek-Mohammadi, H. (2017), "Biaxial buckling analysis of functionally graded nanocomposite sandwich plates reinforced by aggregated carbon nanotube using improved high-order theory", *J. Sandw. Struct. Mater.*, **19**(6), 736-769. https://doi.org/10.1177/1099636216643425.

Nieto, A., Bisht, A., Lahiri, D., Zhang, C. and Agarwal, A. (2017), "Graphene reinforced metal and ceramic matrix composites: A review", *Int. Mater. Rev.*, **62**(5), 241-302. https://doi.org/10.1080/09506608.2016.1219481.

Park, S.K. and Gao, X.L. (2006), "Bernoulli–Euler beam model based on a modified couple stress theory", *J. Micromech. Microeng.*, **16**(11), 2355. https://doi.org/10.1088/0960-1317/16/11/015.

Rakrak, K., Zidour, M., Heireche, H., Bousahla, A.A. and Chemi, A. (2016), "Free vibration analysis of chiral double-walled carbon nanotube using non-local elasticity theory", *Adv. Nano Res., Int. J.*, **4**(1), 31-44. http://dx.doi.org/10.12989/anr.2016.4.1.031.

Reddy, R.M.R., Karunasena, W. and Lokuge, W. (2018), "Free vibration of functionally graded-GPL reinforced composite plates with different boundary conditions", *Aerosp. Sci. Technol.*, **78**, 147-156. https://doi.org/10.1016/j.ast.2018.04.019.

Rostami, R., Mohammadimehr, M., Ghannad, M. and Jalali, A. (2018), "Forced vibration analysis of nano-composite rotating pressurized microbeam reinforced by CNTs based on MCST with temperature-variable material properties", *Theor. Appl. Mech. Lett.*, **8**(2), 97-108. https://doi.org/10.1016/j.taml.2018.02.005.

Sahmani, S. and Aghdam, M.M. (2017), "Nonlocal strain gradient beam model for nonlinear vibration of prebuckled and postbuckled multilayer functionally graded GPLRC nanobeams", *Compos. Struct.*, **179**, 77-88. https://doi.org/10.1016/j.compstruct.2017.07.064.

Semmah, A., Beg, O.A., Mahmoud, S.R., Heireche, H. and Tounsi, A. (2014), "Thermal buckling properties of zigzag single-walled carbon nanotubes using a refined nonlocal model", *Adv. Mater. Res., Int. J.*, **3**(2), 77-89. http://dx.doi.org/10.12989/amr.2014.3.2.077.

Shenas, A.G., Ziaee, S. and Malekzadeh, P. (2018). "A unified higher-order beam theory for free vibration and buckling of FGCNT-reinforced microbeams embedded in elastic medium based on unifying stress–strain gradient framework", *Iran. J. Sci. Technol. Trans. Mech. Eng.*, **43**, 469-492. https://doi.org/10.1007/s40997-018-0171-z.

Tang, C. and Alici, G. (2011), "Evaluation of length-scale effects for mechanical behaviour of micro-and nanocantilevers: II Experimental verification of deflection models using atomic force microscopy", *J. Phys. D Appl. Phys.*, **44**(33), 335502. https://doi.org/10.1088/0022-3727/44/33/335502.

Wang, X., Yang, H., Song, L., Hu, Y., Xing, W. and Lu, H. (2011), "Morphology, mechanical and thermal properties of graphene reinforced poly (butylenesuccinate) nanocomposites", *Compos. Sci. Technol.*, **72**(1), 1-6. https://doi.org/10.1016/j.compscitech.2011.05.007.

Wi, D. and Sodemann, A. (2019), "Investigation of the size effect on the resonant behavior of mesoscale cantilever beams", *J. Vib. Control*, **25**(23-24), 2946-2955. https://doi.org/10.1177/1077546319872311.

Wu, H.L., Yang, J. and Kitipornchai, S. (2016), "Imperfection sensitivity of postbuckling behaviour of functionally graded carbon nanotube-reinforced composite beams", *Thin-Wall. Struct.*, **108**, 225-233. https://doi.org/10.1016/j.tws.2016.08.024.

Yang, J., Wu, H. and Kitipornchai, S. (2017), "Buckling and postbuckling of functionally graded multilayer graphene platelet-reinforced composite beams", *Compos. Struct*., **161**, 111-118. https://doi.org/10.1016/j.compstruct.2016.11.048.

Yazid, M., Heireche, H., Tounsi, A., Bousahla, A.A. and Houari, M.S.A. (2018), "A novel nonlocal refined plate theory for stability response of orthotropic single-layer graphene sheet resting on elastic medium", *Smart Struct. Syst., Int. J.*, **21**(1), 15-25. https://doi.org/10.12989/sss.2018.21.1.015.

Zhao, Z., Feng, C., Wang, Y. and Yang, J. (2017), "Bending and vibration analysis of functionally graded trapezoidal nanocomposite plates reinforced with graphene nanoplatelets (GPLs)", *Compos. Struct.*, **180**, 799-808. https://doi.org/10.1016/j.compstruct.2017.08.044.

CC